Further Results on Bandwidth-Efficient Trellis-Coded Modulation with Prescribed Decoding Delay

M. K. Simon,[1] S. Darden,[1] and M. Fong[1]

Motivated by previous work of Li and Rimoldi for obtaining bandwidth-efficient trellis-coded modulation (TCM) signals with finite decoding delay, we present an alternative representation for their encoder/signal-mapper transmitter structure that consists of merely a single filter (with complex impulse response) having an input equal to the (+1,−1) equivalent of the (0,1) input data bits in their implementation. The filter impulse response is of duration $(\nu+1)/T_b$ (ν is the memory of the modulation, T_b is the bit time, and νT_b is the decoding delay) and can be constructed by designing its $\nu+1$ bit time partitions in terms of the waveform differences that characterize the finite decoding delay conditions found by Li and Rimoldi. The advantage of this simpler transmitter structure is that it readily allows computation of the modulation's power spectral density, from which one can determine the conditions that must be imposed on the signal design to produce an equivalent lowpass power spectral density. This in turn allows for a straightforward procedure for designing the optimum signals to produce maximum bandwidth efficiency as measured by fractional out-of-band power. Such optimum signal designs are determined for memory-one and memory-two modulations and are presented as examples of the application of the general results.

I. Introduction

In a paper presented at the 1997 International Symposium on Information Theory [1], Li and Rimoldi presented a particular transmitter structure (the combination of an encoder of memory ν and a waveform mapper—see Fig. 1) for trellis-coded modulations (TCMs) that, under certain constraints placed on the differences of the transmitted waveforms, guaranteed decoding (using a conventional trellis decoder) with a finite (ν bit duration) delay. Specifically, the encoder was simply a tapped delay line whose ν taps together with the input bit were mapped into a set of $M = 2^{\nu+1}$ waveforms (signals) of 1-bit duration (T_b) in accordance with a binary coded decimal (BCD) relationship. That is, if $U_n \in 0, 1$ denotes the nth input bit and $U_{n-1}, U_{n-2}, \cdots, U_{n-\nu}$ the previous ν bits (the state of the encoder), then the signal transmitted in the interval $nT_b \leq t \leq (n+1)\,T_b$ would be $s_i\,(t)$, where the index i is defined in terms

[1] Communications Systems and Research Section.

The research described in this publication was carried out by the Jet Propulsion Laboratory, California Institute of Technology, under a contract with the National Aeronautics and Space Administration.

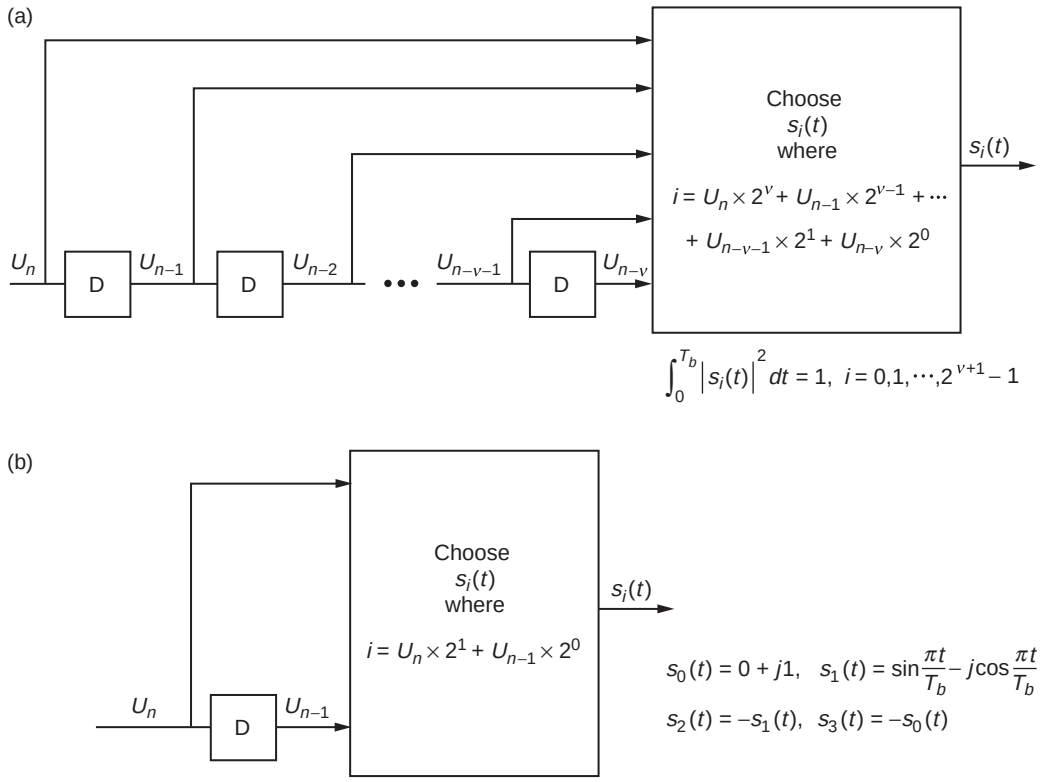

Fig. 1. Transmitter structure: (a) a trellis-coded modulation complex baseband transmitter and (b) the special case of "MSK" ($\nu = 1$).

of these bits by $i = U_n \times 2^{\nu} + U_{n-1} \times 2^{\nu-1} + \cdots + U_{n-\nu-1} \times 2^1 + U_{n-\nu} \times 2^0$. It was also shown in [1] that, in addition to the constraints placed on the waveform differences, it was possible to further constrain the signals so as to maximize the value of the minimum squared Euclidean distance taken over all pairs of error event paths, namely, $d^2_{\min} = 2$. Such a maximum value of $d^2_{\min}$, which corresponds to a number of binary modulations such as binary phase-shift-keying (BPSK) and the more bandwidth efficient minimum-shift-keying (MSK), indicates that the receiver is providing optimum reception from a power conservation standpoint. Finally, in the presence of all of the above constraints, Li and Rimoldi [1] showed that it is possible to further optimize the system by selecting a set of waveforms that minimizes the bandwidth–bit time product, BT_b.

In this article, we investigate an alternative (simpler) representation of the transmitter configuration suggested in [1] that consists of nothing more than a single filter (with complex impulse response) whose input is the ± 1 equivalent of the input data bits, namely, $\bar{U}_n = 1 - 2U_n$ for all n. This representation comes about by viewing the transmitted signal as a random pulse train with a pulse shape that extends beyond a single bit interval, i.e., one that contributes intersymbol interference (ISI) to its neighbors. As we shall see, such a pulse shape of duration $(\nu + 1)\, T_b$ can be constructed by designing its $\nu + 1$ partitions of duration T_b seconds in terms of the waveform differences that are output from Li and Rimoldi's transmitter. Such an ISI-based transmitter representation has the advantage that the power spectral density (PSD) and hence the bandwidth are readily evaluated using known results for uncoded random binary complex pulse trains. It also allows for applying the insight provided in Forney's classic paper [2] on the Viterbi algorithm, in particular the discussion regarding the use of this algorithm to combat ISI, to the trellis decoder (optimum sequence detector), thereby intuitively validating the fact that, for the class of TCMs under investigation, $d^2_{\min} \leq 2$.

One of the requirements placed on the set of possible transmitted waveforms $s_i(t), i = 0, 1, \cdots, M$ in [1] is that they all have equal energy.[2] Following consideration of the alternative representation described above, we investigate the impact of relaxing the equal-energy restriction on the power efficiency of the modulation scheme in its ability to achieve the largest value of $d^2_{\min}$. In particular, we propose an additional set of constraints (now on the differences of the *energies* of the signals) that must be satisfied to achieve the same finite decoding delay, using again the optimum sequence receiver, and then demonstrate that such a set of constraints results in a signal design with a maximum value of $d^2_{\min}$ less than two. Allowing the signals to have unequal energy, however, suggests the possibility of additional flexibility in the design of these signals in order to achieve the best bandwidth efficiency. Thus, the reduction in $d^2_{\min}$ caused by the unequal energy requirement can possibly trade off against an additional reduction in signal bandwidth. Additional consideration of this notion warrants investigation.

II. ISI-Based Transmitter Implementation

The decomposition of a memory modulation into a cascade of an encoder and a memoryless modulator was first applied to continuous phase modulation (CPM) by Rimoldi [3]. In particular, for MSK, a special case of CPM corresponding to a rectangular frequency pulse of duration T_b seconds (full response) and frequency-modulation index (two-sided frequency deviation normalized by the bit rate) $h = 0.5$, the memory is $\nu = 1$, and a transmitter analogous to Fig. 1 was obtained, as in Fig. 2. Comparing Figs. 1 and 2, we note that in the latter the state is represented by the *differentially encoded* version of the current input bit $V_n = U_n \oplus V_{n-1}$, whereas in the former it would be just the previous input bit U_{n-1} itself. Furthermore, because of the differential encoding associated with the state in Fig. 2, a differential decoder would be required in the receiver following the trellis decoder, which results in a small loss in bit-error probability (BEP) performance. It is well known [4, Chapter 10] that precoding true MSK with a differential decoder at the transmitter results in a modulation that is equivalent (spectral and power efficiently) to MSK but without the need for differential decoding at the receiver. It is such precoded MSK that is implemented by the simpler configuration of Fig. 1. In what follows, when referring to MSK in the context of Fig. 1(b) or its equivalents, we shall assume that precoded MSK is what is implied, as represented by the quotation marks around MSK in the caption.

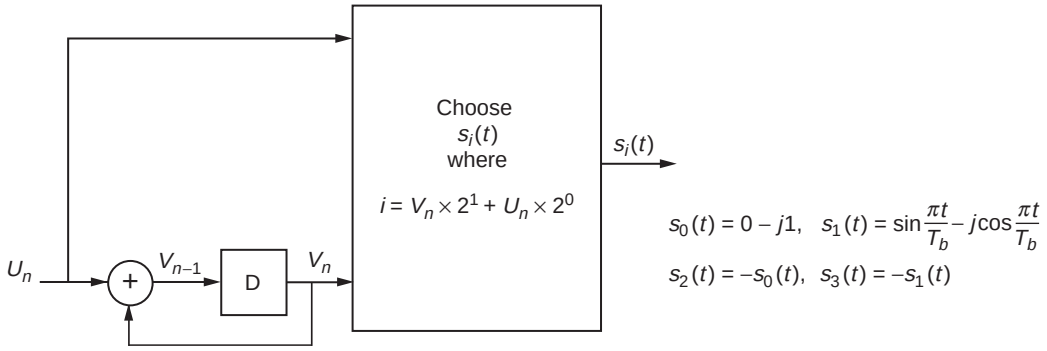

Fig. 2. Trellis-coded modulation complex baseband transmitter for MSK based on Rimoldi decomposition of CPM.

[2] Note that the assumption of equal energy does not imply constant envelope, as was the case for the continuous phase modulations (CPMs) studied in [3] that served as the motivation for the work leading up to the results in [1]. Nevertheless, the envelope fluctuation of the resulting signal designs will be small when compared with Nyquist designs of comparable bandwidth efficiencies.

Consider an uncoded random binary (± 1) sequence $\left\{\bar{U}_n\right\}$ that generates a random pulse train

$$s(t) = \sum_{n=-\infty}^{\infty} \bar{U}_n p(t - nT_b) \tag{1}$$

where $p(t) \triangleq p_R(t) + jp_I(t)$ is a complex pulse shape defined on the interval $0 \le t \le (\nu+1)T_b$. Consider partitioning $p(t)$ into $\nu+1$ adjoint pieces corresponding to its 1-bit interval sections. That is, we define the set of T_b-second duration waveforms

$$p_k(t) \triangleq p_{Rk}(t) + jp_{Ik}(t) = \begin{cases} p(t+kT), & 0 \le t \le T_b \\ 0, & \text{otherwise} \end{cases}, \quad k = 0, 1, 2, \cdots, \nu \tag{2}$$

From Eq. (1), in any T_b-second interval, e.g., the nth, the signal $s(t)$ will be described by one of $M = 2^{\nu+1}$ complex waveforms, i.e., $s_k(t - nT_b)$, $k = 0, 1, 2, \cdots, 2^{\nu+1} - 1$, which are expressed in terms of $p(t)$ and the data sequence $\left\{\bar{U}_n\right\}$ by

$$s_k(t - nT_b) = \bar{U}_n p_0(t - nT_b) + \bar{U}_{n-1} p_1(t - nT_b) + \cdots + \bar{U}_{n-\nu} p_\nu(t - nT_b), \quad k = 0, 1, 2, \cdots, 2^{\nu+1} - 1 \tag{3}$$

where the index k is the equivalent (0,1) bit sequence $\{U_n, U_{n-1}, \cdots, U_{n-\nu}\}$ expressed in BCD form. As an example, the set of waveforms for memory $\nu = 2$ is given below:

$$\left.\begin{aligned}
s_0(t - nT_b) &= p_0(t - nT_b) + p_1(t - nT_b) + p_2(t - nT_b) \\
s_1(t - nT_b) &= p_0(t - nT_b) + p_1(t - nT_b) - p_2(t - nT_b) \\
s_2(t - nT_b) &= p_0(t - nT_b) - p_1(t - nT_b) + p_2(t - nT_b) \\
s_3(t - nT_b) &= p_0(t - nT_b) - p_1(t - nT_b) - p_2(t - nT_b) \\
s_4(t - nT_b) &= -p_0(t - nT_b) + p_1(t - nT_b) + p_2(t - nT_b) \\
s_5(t - nT_b) &= -p_0(t - nT_b) + p_1(t - nT_b) - p_2(t - nT_b) \\
s_6(t - nT_b) &= -p_0(t - nT_b) - p_1(t - nT_b) + p_2(t - nT_b) \\
s_7(t - nT_b) &= -p_0(t - nT_b) - p_1(t - nT_b) - p_2(t - nT_b)
\end{aligned}\right\} \tag{4}$$

We note from Eq. (4) that, because of the BCD construction, the following properties hold for the signal differences:

$$s_0(t) - s_1(t) = s_2(t) - s_3(t) = s_4(t) - s_5(t) = s_6(t) - s_7(t) = 2p_2(t) \tag{5a}$$

$$s_0(t) - s_2(t) = s_4(t) - s_6(t) = 2p_1(t) \tag{5b}$$

Also, an equivalent (at least in so far as the first equality is concerned) condition to Eq. (5b) is

$$s_0(t) - s_4(t) = s_2(t) - s_6(t) = 2p_0(t) \tag{5c}$$

In the more generic case for arbitrary ν, the representations of the signals $s_0(t)$ and $s_{2^m}(t)$, $m = 0, 1, 2, \cdots, \nu-1$ as in Eq. (3) differ only in the bit position corresponding to $p_{\nu-m}(t)$. A similar statement can be made for the signals $s_{2^{m+1}l}(t)$ and $s_{2^{m+1}l+2^m}(t)$, $m = 0, 1, 2, \cdots, \nu-1$, $l = 1, 2, \cdots, 2^{\nu-m}-1$. Thus, the conditions corresponding to Eqs. (5a) and (5b) would be generalized as

$$s_0(t) - s_{2^m}(t) = s_{2^{m+1}l}(t) - s_{2^{m+1}l+2^m}(t) = 2p_{\nu-m}(t), \quad m = 0, 1, 2, \cdots, \nu-1, \quad l = 1, 2, \ldots, 2^{\nu-m}-1 \tag{6}$$

and in addition the generalization of Eq. (5c) becomes

$$s_0(t) - s_{2^\nu}(t) = s_{2^{\nu-1}}(t) - s_{2^\nu+2^{\nu-1}}(t) = 2p_0(t) \tag{7}$$

The conditions on the signal differences of $s_i(t)$ given in Eq. (6) are precisely those of Theorem I in [1], which guarantees a finite decoding delay of ν bits using an optimum trellis-coded receiver.[3] Therefore, since $p(t)$ is entirely specified by its adjoint T_b-second sections $p_i(t)$, $i = 0, 1, \cdots, \nu$, we see that the transmitter of Fig. 1(a) can be equivalently implemented (see Fig. 3) by passing the input ± 1 data sequence $\{\bar{U}_n\}$ (modeled as a random impulse train) through a filter with complex impulse response

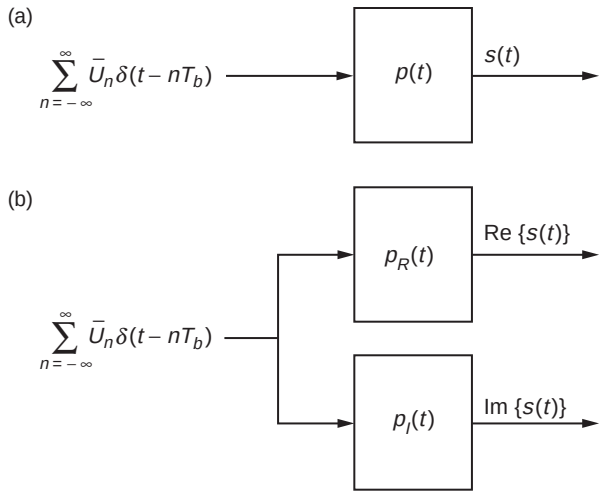

Fig. 3. Transmitter structure equivalent to Fig. 1(a): (a) complex baseband form and (b) I–Q baseband form.

[3] It has also been noted by Li and Rimoldi that these conditions guarantee that the Euclidean distance between any pair of paths in the trellis decoder that diverge at time n and remerge at time $n+\nu+1$ is the same. Furthermore, the number of correlators (matched filters) needed to implement the optimum MLSE receiver will now vary *linearly* with memory, i.e., $\nu+1$, as opposed to *exponentially* with memory, i.e., $2^{\nu+1}$, which is the case when no constraints are imposed on the decoding delay.

$$\left.\begin{aligned} p(t) &= \sum_{i=0}^{\nu} p_i(t - iT_b) \\ p_i(t) &= \frac{1}{2}\left[s_0(t) - s_{2^{\nu-i}}(t)\right] \end{aligned}\right\} \tag{8}$$

Equivalently, the real and imaginary parts of the baseband signal (to be modulated onto quadrature carriers for transmission over the channel) can be obtained by passing the common input ± 1 data sequence $\{\bar{U}_n\}$ through a pair of filters with respective impulse responses

$$\left.\begin{aligned} p_{Ri}(t) &= \frac{1}{2}\left[s_{R0}(t) - s_{R2^{\nu-i}}(t)\right] \\ p_{Ii}(t) &= \frac{1}{2}\left[s_{I0}(t) - s_{I2^{\nu-i}}(t)\right] \end{aligned}\right\} \tag{9}$$

Note that $p_R(t)$ and $p_I(t)$ as constructed from the components in Eq. (9) do not necessarily have equal energy. We shall see that this is true even for the simple case of MSK. It is further interesting to note that the signals of Eq. (4) also satisfy the conditions

$$\left.\begin{aligned} s_0(t) &= -s_7(t) \\ s_1(t) &= -s_6(t) \\ s_2(t) &= -s_5(t) \\ s_3(t) &= -s_4(t) \end{aligned}\right\} \tag{10}$$

or in the case of arbitrary memory ν,

$$s_m(t) = -s_{2^{\nu+1}-1-m}(t), \quad m = 0, 1, \cdots, 2^{\nu} - 1 \tag{11}$$

The conditions of Eq. (11) are precisely those given in [1] that achieve the maximum value of minimum squared Euclidean distance, namely, $d^2_{\min} = 2$. Thus, the implementation of Fig. 3 not only achieves finite decoding delay but also automatically achieves the optimum performance from the standpoint of power efficiency. This result should not be surprising in view of the findings in [2], which indicate that a maximum-likelihood (optimum) sequence estimator (MLSE) form of receiver such as the trellis decoder can completely remove the ISI and thereby achieve the performance of a zero-ISI (full-response) system.

What remains is to consider the bandwidth efficiency of signals designed according to the constraints of Eqs. (6), (7), and (11). This is where the ISI-based representation of Fig. 3 helps considerably since the evaluation of the PSD of the transmitted signal can be trivially accomplished using well-known relations [4] for random pulse trains. This is considered in the next section.

III. Evaluation of the Power Spectral Density

In this section, we compute the PSD of a random complex pulse train, e.g., that in Eq. (1), modulated onto quadrature carriers. That is, if the transmitted bandpass signal is given by[4]

$$\tilde{s}(t) = \mathrm{Re}\left\{s(t)\, e^{j2\pi f_m t}\right\} = \left(\sum_{n=-\infty}^{\infty} \bar{U}_n p_R(t - nT_b)\right)\cos 2\pi f_m t - \left(\sum_{n=-\infty}^{\infty} \bar{U}_n p_I(t - nT_b)\right)\sin 2\pi f_m t \quad (12)$$

then it is straightforward to show, using an extension of the methods in [4, Chapter 2], that the PSD of $\tilde{s}(t)$ is given by

$$\begin{aligned} S(f) &= \frac{1}{4T_b}\left|P_R(f - f_m) + jP_I(f - f_m)\right|^2 + \frac{1}{4T_b}\left|P_R(f + f_m) - jP_I(f + f_m)\right|^2 \\ &= \frac{1}{4T_b}\left|P(f - f_m)\right|^2 + \frac{1}{4T_b}\left|P(-f - f_m)\right|^2 \triangleq S_u(f) + S_l(f) \end{aligned} \quad (13)$$

where

$$\left.\begin{aligned} P_R(f) &\triangleq \mathcal{F}\{p_R(t)\} \\ P_R(f) &\triangleq \mathcal{F}\{p_I(t)\} \\ P(f) &\triangleq \mathcal{F}\{p(t)\} \end{aligned}\right\} \quad (14)$$

are the Fourier transforms of the corresponding pulse shapes and, in general, are complex functions of f, and the u and l subscripts denote the upper and lower sidebands, respectively. Note that the signal in Eq. (12) differs from the usual quadrature phase-shift-keying (QPSK) type of signal in that here the same data sequence is passed through both the in-phase (I) and quadrature (Q) filters, whereas for QPSK the two sequences passing through these filters would be different and independent of one another. As such, the PSD in Eq. (13) cannot, in general, be written in the form [4, Chapter 2, Eq. (2.131)]

$$S(f) = \frac{1}{4}G(f - f_c) + \frac{1}{4}G(f + f_c) \quad (15)$$

where $G(f)$ is the equivalent baseband (symmetrical around $f = 0$) PSD and is a real function of f, and f_c is some arbitrary carrier frequency.[5]

---

[4] We use the notation "f_m" for the actual modulating frequency of the quadrature carriers to distinguish it from the carrier frequency around which the PSD is symmetric, which will be denoted by "f_c." More about this shortly.

[5] What is meant here by an "equivalent baseband PSD" is a PSD around zero frequency that is *identical* to the upper or lower sideband of the bandpass PSD frequency shifted to the origin. While it is always possible to express Eq. (13) in the form $S(f) = (1/4)G_u(f - f_c) + (1/4)G_l(f + f_c)$, where $G_u(f) = G_l(-f)$, in general, there is no guarantee that $G_u(f)$ [or equivalently, $G_l(f)$] has symmetry about the origin or, for that matter, about any frequency f_c. Stated another way, while demodulating the bandpass signal with a carrier at some frequency f_c (not necessarily equal to the modulating frequency f_m) will always produce a symmetric PSD around the origin, the resulting baseband PSD will, in general, be a combination (sum) of the aliased upper and lower sidebands, and may or may not appear as a simple frequency translation of either of these sidebands.

To illustrate the above point, consider the specific case of MSK ($\nu = 1$) for which the four complex signals are given by[6]

$$\left.\begin{aligned} s_0(t) &= 0 + j1 \\ s_1(t) &= \sin\frac{\pi t}{T_b} - j\cos\frac{\pi t}{T_b} = s_0^*(t)\, e^{j(\pi t/T_b)} \\ s_2(t) &= -s_1(t) \\ s_3(t) &= -s_0(t) \end{aligned}\right\} \tag{16}$$

In terms of the ISI-based representation, we obtain from Eq. (8) that

$$\left.\begin{aligned} p_0(t) &= \frac{1}{2}\sin\frac{\pi t}{T_b} + j\frac{1}{2}\left[1 - \cos\frac{\pi t}{T_b}\right] \\ p_1(t) &= -\frac{1}{2}\sin\frac{\pi t}{T_b} + j\frac{1}{2}\left[1 + \cos\frac{\pi t}{T_b}\right] \end{aligned}\right\} \tag{17}$$

Thus, using Eq. (17) to define the complex pulse shape of Eq. (8), we obtain

$$p(t) = \frac{1}{2}\sin\frac{\pi t}{T_b} + j\frac{1}{2}\left[1 - \cos\frac{\pi t}{T_b}\right], \quad 0 \le t \le 2T_b \tag{18}$$

That is, an appropriate implementation for MSK that guarantees a decoding delay of 1 bit is that of Fig. 3 with I and Q filters having impulse responses

$$\left.\begin{aligned} p_R(t) &= \frac{1}{2}\sin\frac{\pi t}{T_b}, \quad 0 \le t \le 2T_b \\ p_I(t) &= \frac{1}{2}\left[1 - \cos\frac{\pi t}{T_b}\right], \quad 0 \le t \le 2T_b \end{aligned}\right\} \tag{19}$$

Taking the Fourier transforms of $p_R(t)$ and $p_I(t)$ of Eq. (8) and using these in Eq. (13), we arrive at the following result for the bandpass PSD:

---

[6] Note that, for the Rimoldi decomposition of MSK illustrated in Fig. 2, the signals satisfy the condition $s_0(t) - s_1(t) = -(s_2(t) - s_3(t))$ rather than $s_0(t) - s_1(t) = s_2(t) - s_3(t)$ as in Eq. (5a).

$$S(f) = \frac{T_b}{4}\frac{\sin^2 2\pi (f-f_m)T_b}{\pi^2}\left[\frac{1}{1-2(f-f_m)T_b} + \frac{1}{2(f-f_m)T_b}\right]^2$$

$$+ \frac{T_b}{4}\frac{\sin^2 2\pi (f+f_m)T_b}{\pi^2}\left[\frac{1}{1+2(f+f_m)T_b} - \frac{1}{2(f+f_m)T_b}\right]^2$$

$$= S_u(f) + S_l(f) \tag{20}$$

Note that while $S(f)$ is an even function of f (as it should be for a real signal), its upper and lower sidebands, $S_u(f)$ and $S_l(f)$, are not symmetric around f_m and $-f_m$, respectively. However, there does exist a frequency, $f_c \neq f_m$, around which the upper sideband (and similarly for the lower sideband) is symmetric. To understand why this is so, we remind the reader that, according to Rimoldi's decomposition [3], the modulation frequency chosen for the quadrature carriers should be shifted from the carrier frequency f_c around which the bandpass spectrum is to be symmetric by an amount equal to $1/4T_b$, i.e., $f_m = f_c - 1/4T_b$. The reason for this stems from the fact that the specification of the signals as in Eq. (16) results in a tilted trellis where the phase tilt is equal to $\pi/2$ rad. (Note that a frequency shift of $\Delta f = 1/4T_b$ is equal to a phase shift $2\pi\Delta f T_b = \pi/2$.) To demonstrate that this is indeed the case, we evaluate the PSD of MSK using Eq. (20) with the shifted value of modulating frequency $f_m = f_c - 1/4T_b$. When this is done, the result in Eq. (15) is obtained with

$$G(f) = \frac{16T_b}{\pi^2}\frac{\cos^2 2\pi f T_b}{\left(1-16f^2T_b^2\right)^2} \tag{21}$$

which corresponds (except for a normalization factor) to the well-know PSD of MSK [4, Chapter 2, Eq. (2.148)].

The question that comes about now is: For arbitrary memory ν and a baseband signal design satisfying Eqs. (6), (7), and (11), is it possible to find a modulating frequency f_m that will produce a symmetric bandpass PSD around some carrier frequency f_c? If not, then one cannot find an equivalent baseband PSD in the sense of Footnote 5 and hence the bandwidth (whatever measure is used) of the signal must be determined from the RF waveform. To shed some light on the answer to this question, we consider the simplest case of unit memory, where the complex pulse shape of Eq. (8) is simply given by

$$p(t) = \frac{1}{2}\left[s_0(t) - s_2(t) + s_0(t-T_b) - s_1(t-T_b)\right]$$

$$= \frac{1}{2}\left[s_0(t) + s_0(t-T_b) + s_1(t) + s_2(t-T_b)\right], \quad 0 \le t \le 2T_b \tag{22}$$

where, in accordance with Eq. (11), we have used the fact that $s_1(t) = -s_2(t)$ in order to achieve $d^2_{\min} = 2$. The Fourier transform of $p(t)$ in Eq. (22) is given by

$$P(f) = \frac{1}{2}\left[\int_0^{T_b} s_0(t)\left(1+e^{-j2\pi f T_b}\right)e^{-j2\pi f t}dt + \int_0^{T_b} s_1(t)\,e^{-j2\pi f t}dt + e^{-j2\pi f T_b}\int_0^{T_b} s_2(t)\,e^{-j2\pi f t}dt\right] \tag{23}$$

Since from Eq. (13) the upper spectral sideband is $S_u(f) = (1/4T_b)\left|P(f-f_m)\right|^2$, then, in order for this to be symmetric around f_c, we must have

$$\left|P\left(f_c+f-f_m\right)\right|^2=\left|P\left(f_c-f-f_m\right)\right|^2 \tag{24}$$

or, letting $f_s \triangleq f_c-f_m$ denote the separation between the actual modulation frequency and the bandpass frequency around which symmetry is desired, $s_0\left(t\right)$ and $s_1\left(t\right)$ must be chosen to satisfy

$$\left|P\left(f_s+f\right)\right|^2=\left|P\left(f_s-f\right)\right|^2 \tag{25a}$$

or equivalently

$$\left|P\left(f_s+f\right)\right|^2=\left|P^*\left(f_s-f\right)\right|^2 \tag{25b}$$

for some f_s. In terms of Eq. (23), the spectral equality in Eq. (25b) requires that we have

$$\begin{aligned}
&\left|\int_0^{T_b}\left(s_0(t)e^{-j2\pi f_s t}\right)e^{-j2\pi ft}dt+e^{-j2\pi(f_s+f)T_b}\int_0^{T_b}\left(s_0(t)e^{-j2\pi f_s t}\right)e^{-j2\pi ft}dt\right.\\
&\quad\left.+\int_0^{T_b}\left(s_1(t)e^{-j2\pi f_s t}\right)e^{-j2\pi ft}dt+e^{-j2\pi(f_s+f)T_b}\int_0^{T_b}\left(s_2(t)e^{-j2\pi f_s t}\right)e^{-j2\pi ft}dt\right|^2\\
&=\left|\int_0^{T_b}\left(s_0^*(t)e^{j2\pi f_s t}\right)e^{-j2\pi ft}dt+e^{j2\pi(f_s-f)T_b}\int_0^{T_b}\left(s_0^*(t)e^{j2\pi f_s t}\right)e^{-j2\pi ft}dt\right.\\
&\quad\left.+\int_0^{T_b}\left(s_1^*(t)e^{j2\pi f_s t}\right)e^{-j2\pi ft}dt+e^{j2\pi(f_s-f)T_b}\int_0^{T_b}\left(s_2^*(t)e^{j2\pi f_s t}\right)e^{-j2\pi ft}dt\right|^2
\end{aligned} \tag{26}$$

Sufficient conditions on the signals $\{s_i\left(t\right)\}$ for Eq. (26) to be satisfied are

$$\left.\begin{aligned}
s_1\left(t\right)&=s_0^*\left(t\right)e^{j4\pi f_s t}\\
s_2\left(t\right)&=e^{j4\pi f_s T_b}s_0^*\left(t\right)e^{j4\pi f_s t}
\end{aligned}\right\} \tag{27}$$

However, since in arriving at Eq. (26) we have already assumed that $s_1\left(t\right)=-s_2\left(t\right)$, then Eq. (27) further requires that $f_s=1/4T_b$, from which we obtain the complete signal set

$$\left.\begin{aligned}
s_1\left(t\right)&=s_0^*\left(t\right)e^{j\pi t/T_b}\\
s_2\left(t\right)&=-s_0^*\left(t\right)e^{j\pi t/T_b}\\
s_3\left(t\right)&=-s_0\left(t\right)
\end{aligned}\right\} \tag{28}$$

Note that for memory one it is necessary to specify only $s_0(t)$ in order to arrive at the complete signal set. Also, the signal set of Eq. (28) satisfies the finite decoding delay condition of [1], namely, $s_0(t) - s_1(t) = s_2(t) - s_3(t)$.

The equivalent lowpass PSD is obtained by first using $s_1(t) = -s_2(t)$ in Eq. (23), resulting in

$$\begin{aligned} P(f) &= \frac{1}{2}\left[\int_0^{T_b} \big(s_0(t) + s_1(t)\big)e^{-j2\pi ft}dt + e^{-j2\pi fT_b}\int_0^{T_b} \big(s_0(t) - s_1(t)\big)e^{-j2\pi ft}dt\right] \\ &= \frac{1}{2}\left[S_0(f) + S_1(f) + e^{-j2\pi fT_b}\big(S_0(f) - S_1(f)\big)\right] \end{aligned} \tag{29}$$

from which one immediately gets

$$\begin{aligned} \frac{1}{T_b}\big|P(f)\big|^2 &= \frac{1}{4T_b}\Big[\big|S_0(f) + S_1(f)\big|^2 + \big|e^{-j2\pi fT_b}\big(S_0(f) - S_1(f)\big)\big|^2 \\ &\quad + 2\,\mathrm{Re}\Big\{\big(S_0^*(f) + S_1^*(f)\big)\big(S_0(f) - S_1(f)\big)e^{-j2\pi fT_b}\Big\}\Big] \\ &= \frac{1}{2T_b}\Big[\big|S_0(f)\big|^2 + \big|S_1(f)\big|^2 + \mathrm{Re}\Big\{\big(S_0^*(f) + S_1^*(f)\big)\big(S_0(f) - S_1(f)\big)e^{-j2\pi fT_b}\Big\}\Big] \end{aligned} \tag{30}$$

In Eqs. (29) and (30), $S_i(f)$ denotes the Fourier transform of $s_i(t)$. Using the first symmetry condition of Eq. (28) in Eq. (30) gives the desired equivalent lowpass PSD, namely,

$$\begin{aligned} &\frac{1}{T_b}\left|P\left(f+\frac{1}{4T_b}\right)\right|^2 \\ &= \frac{1}{2T_b}\left[\left|S_0\left(f+\frac{1}{4T_b}\right)\right|^2 + \left|S_0\left(-f+\frac{1}{4T_b}\right)\right|^2\right. \\ &\quad \left. +\mathrm{Im}\left\{\left(S_0^*\left(f+\frac{1}{4T_b}\right) + S_0\left(-f+\frac{1}{4T_b}\right)\right)\left(S_0\left(f+\frac{1}{4T_b}\right) - S_0^*\left(-f+\frac{1}{4T_b}\right)\right)e^{-j2\pi fT_b}\right\}\right] \\ &= \left|S_0\left(f+\frac{1}{4T_b}\right)\right|^2[1-\sin 2\pi fT_b] + \left|S_0\left(-f+\frac{1}{4T_b}\right)\right|^2[1+\sin 2\pi fT_b] \\ &\quad + 2\left[\mathrm{Re}\left\{S_0\left(f+\frac{1}{4T_b}\right)\right\}\mathrm{Im}\left\{S_0\left(-f+\frac{1}{4T_b}\right)\right\}\right. \\ &\quad \left. +\mathrm{Re}\left\{S_0\left(-f+\frac{1}{4T_b}\right)\right\}\mathrm{Im}\left\{S_0\left(f+\frac{1}{4T_b}\right)\right\}\right]\cos 2\pi fT_b \end{aligned} \tag{31}$$

which is clearly an even function of frequency.

Although Eq. (28) is satisfied by the MSK signals of Eq. (16), as should be the case, this condition applies in a more general context since it does not explicitly specify $s_0(t)$ but rather only the *relation between* $s_0(t)$ and $s_1(t)$. This should not be surprising since it has been shown in the past that there exists an entire class of MSK-type signals (referred to in [5] as generalized MSK) that happen to also be constant envelope (in addition to being equal energy) and that achieve $d^2_{\min} = 2$ as well as a decoding delay of 1-bit interval. To illustrate the point, consider the class of binary full-response CPM signals with modulation index $h = 1/2$ and equivalent phase pulse $f(t)$, which satisfies the conditions $f(0) = 0, f(T_b) = 1/2$. A specific example of such a signal is Amoroso's sinusoidal frequency-shift keying (SFSK) [6] for which

$$f(t) = \frac{t}{2T_b}\left(1 - \frac{\sin 2\pi t/T_b}{2\pi t/T_b}\right), \quad 0 \le t \le T_b \tag{32}$$

corresponding to a raised-cosine *frequency* pulse

$$g(t) = \frac{df(t)}{dt} = \frac{1}{2T_b}\left(1 - \cos\frac{2\pi t}{T_b}\right), \quad 0 \le t \le T_b \tag{33}$$

Analogously to Eq. (16), the set of signals that satisfy Eq. (27) are now

$$\left.\begin{aligned} s_0(t) &= \sin\left(\pi\left(f(t) - \frac{t}{2T_b}\right)\right) + j\cos\left(\pi\left(f(t) - \frac{t}{2T_b}\right)\right) \\ s_1(t) &= \sin\left(\pi\left(f(t) + \frac{t}{2T_b}\right)\right) - j\cos\left(\pi\left(f(t) + \frac{t}{2T_b}\right)\right) = s_0^*(t)\, e^{j(\pi t/T_b)} \\ s_2(t) &= -s_1(t) \\ s_3(t) &= -s_0(t) \end{aligned}\right\} \tag{34}$$

(Note that Eq. (34) reduces to Eq. (16) for MSK itself when $f(t) = t/2T_b,\ 0 \le t \le T_b$, and $g(t) = 1/2T_b,\ 0 \le t \le T_b$.) For SFSK, Eq. (34) takes the specific form

$$\left.\begin{aligned} s_0(t) &= \sin\left(\frac{\pi t}{2T_b}\left(\frac{\sin 2\pi t/T_b}{2\pi t/T_b}\right)\right) + j\cos\left(\frac{\pi t}{2T_b}\left(\frac{\sin 2\pi t/T_b}{2\pi t/T_b}\right)\right) \\ s_1(t) &= \sin\left(\frac{\pi t}{T_b}\left(1 - \frac{1}{2}\,\frac{\sin 2\pi t/T_b}{2\pi t/T_b}\right)\right) - j\cos\left(\frac{\pi t}{T_b}\left(1 - \frac{1}{2}\,\frac{\sin 2\pi t/T_b}{2\pi t/T_b}\right)\right) \\ s_2(t) &= -s_1(t) \\ s_3(t) &= -s_0(t) \end{aligned}\right\} \tag{35}$$

For memory two, the pulse shape is given by

$$p\left(t\right)=\frac{1}{2}\left[s_0\left(t\right)-s_4\left(t\right)+s_0\left(t-T_b\right)-s_2\left(t-T_b\right)+s_0\left(t-2T_b\right)-s_1\left(t-2T_b\right)\right]$$

$$=\frac{1}{2}\left[s_0\left(t\right)+s_0\left(t-T_b\right)+s_0\left(t-2T_b\right)+s_3\left(t\right)-s_2\left(t-T_b\right)-s_1\left(t-2T_b\right)\right],\quad 0\leq t\leq 3T_b \tag{36}$$

with Fourier transform

$$P(f)=\frac{1}{2}\left[\left(1+e^{-j2\pi fT_b}+e^{-j4\pi fT_b}\right)\int_0^{T_b}s_0(t)e^{-j2\pi ft}dt+\int_0^{T_b}s_3(t)e^{-j2\pi ft}dt\right.$$

$$\left.-e^{-j2\pi fT_b}\int_0^{T_b}s_2(t)e^{-j2\pi ft}dt-e^{-j4\pi fT_b}\int_0^{T_b}s_1(t)e^{-j2\pi ft}dt\right] \tag{37}$$

Applying Eq. (37) to Eq. (25b), we obtain the bandpass spectral symmetry condition

$$\left|\int_0^{T_b}\left(s_0(t)e^{-j2\pi f_st}\right)e^{-j2\pi ft}dt+e^{-j2\pi(f_s+f)T_b}\int_0^{T_b}\left(s_0(t)e^{-j2\pi f_st}\right)e^{-j2\pi ft}dt+e^{-j4\pi(f_s+f)T_b}\right.$$

$$\times\int_0^{T_b}\left(s_0(t)e^{-j2\pi f_st}\right)e^{-j2\pi ft}dt+\int_0^{T_b}\left(s_3(t)e^{-j2\pi f_st}\right)e^{-j2\pi ft}dt-e^{-j2\pi(f_s+f)T_b}$$

$$\left.\times\int_0^{T_b}\left(s_2(t)e^{-j2\pi f_st}\right)e^{-j2\pi ft}dt-e^{-j4\pi(f_s+f)T_b}\int_0^{T_b}\left(s_1(t)e^{-j2\pi f_st}\right)e^{-j2\pi ft}dt\right|^2$$

$$=\left|\int_0^{T_b}\left(s_0^*(t)e^{j2\pi f_st}\right)e^{-j2\pi ft}dt+e^{j2\pi(f_s-f)T_b}\int_0^{T_b}\left(s_0^*(t)e^{j2\pi f_st}\right)e^{-j2\pi ft}dt+e^{j4\pi(f_s-f)T_b}\right.$$

$$\times\int_0^{T_b}\left(s_0^*(t)e^{j2\pi f_st}\right)e^{-j2\pi ft}dt+\int_0^{T_b}\left(s_3^*(t)e^{j2\pi f_st}\right)e^{-j2\pi ft}dt-e^{j2\pi(f_s-f)T_b}$$

$$\left.\times\int_0^{T_b}\left(s_2^*(t)e^{j2\pi f_st}\right)e^{-j2\pi ft}dt-e^{j4\pi(f_s-f)T_b}\int_0^{T_b}\left(s_1^*(t)e^{j2\pi f_st}\right)e^{-j2\pi ft}dt\right|^2 \tag{38a}$$

or, letting $s_3\left(t\right)=s_2\left(t\right)-s_0\left(t\right)+s_1\left(t\right)$ in accordance with Eq. (5a),

$$\left| e^{-j2\pi(f_s+f)T_b} \int_0^{T_b} \left(s_0(t)\, e^{-j2\pi f_s t}\right) e^{-j2\pi f t} dt + e^{-j4\pi(f_s+f)T_b} \int_0^{T_b} \left(s_0(t)\, e^{-j2\pi f_s t}\right) e^{-j2\pi f t} dt \right.$$

$$+ \int_0^{T_b} \left(s_2(t)\, e^{-j2\pi f_s t}\right) e^{-j2\pi f t} dt - e^{-j2\pi(f_s+f)T_b} \int_0^{T_b} \left(s_2(t)\, e^{-j2\pi f_s t}\right) e^{-j2\pi f t} dt$$

$$\left. + \int_0^{T_b} \left(s_1(t)\, e^{-j2\pi f_s t}\right) e^{-j2\pi f t} dt - e^{-j4\pi(f_s+f)T_b} \int_0^{T_b} \left(s_1(t)\, e^{-j2\pi f_s t}\right) e^{-j2\pi f t} dt \right|^2$$

$$= \left| e^{j2\pi(f_s-f)T_b} \int_0^{T_b} \left(s_0^*(t)\, e^{j2\pi f_s t}\right) e^{-j2\pi f t} dt + e^{j4\pi(f_s-f)T_b} \int_0^{T_b} \left(s_0^*(t)\, e^{j2\pi f_s t}\right) e^{-j2\pi f t} dt \right.$$

$$+ \int_0^{T_b} \left(s_2^*(t)\, e^{j2\pi f_s t}\right) e^{-j2\pi f t} dt - e^{j2\pi(f_s-f)T_b} \int_0^{T_b} \left(s_2^*(t)\, e^{j2\pi f_s t}\right) e^{-j2\pi f t} dt$$

$$\left. + \int_0^{T_b} \left(s_1^*(t)\, e^{j2\pi f_s t}\right) e^{-j2\pi f t} dt - e^{j4\pi(f_s-f)T_b} \int_0^{T_b} \left(s_1^*(t)\, e^{j2\pi f_s t}\right) e^{-j2\pi f t} dt \right|^2 \tag{38b}$$

Analogously with Eq. (27), satisfying Eq. (38b) implies the set of conditions

$$s_1(t) + s_2(t) = \left(s_1^*(t) + s_2^*(t)\right) e^{j4\pi f_s t} \tag{39a}$$

$$s_0(t) - s_2(t) = e^{j4\pi f_s T_b} \left(s_0^*(t) - s_2^*(t)\right) e^{j4\pi f_s t} \tag{39b}$$

$$s_0(t) - s_1(t) = e^{j8\pi f_s T_b} \left(s_0^*(t) - s_1^*(t)\right) e^{j4\pi f_s t} \tag{39c}$$

Again letting $f_s = 1/4T_b$ and summing Eqs. (39a), (39b), and (39c) gives

$$s_1(t) + s_2(t) = \left(s_1^*(t) + s_2^*(t)\right) e^{j\pi t/T_b} \tag{40a}$$

$$s_0(t) = s_2^*(t)\, e^{j\pi t/T_b} \quad \left(\text{or equivalently, } s_2(t) = s_0^*(t)\, e^{j\pi t/T_b}\right) \tag{40b}$$

$$s_0(t) - s_1(t) = \left(s_0^*(t) - s_1^*(t)\right) e^{j\pi t/T_b} \tag{40c}$$

Actually, Eq. (40c) is not an independent condition since it can be derived from Eqs. (40a) and (40b). Thus, Eqs. (40a) and (40b) are sufficient to determine the signal design. Expressing the signals in terms of their real and imaginary parts, i.e., $s_i(t) = s_{iR}(t) + j s_{iI}(t)\,,\ i = 0, 1, \cdots, 3$, then Eqs. (40a) and (40c) can alternatively be written as

$$\left(s_{1R}(t)+s_{2R}(t)\right)\left(1-\cos\frac{\pi t}{T_b}\right)=\left(s_{1I}(t)+s_{2I}(t)\right)\sin\frac{\pi t}{T_b} \tag{41a}$$

$$\left(s_{0R}(t)-s_{1R}(t)\right)\left(1-\cos\frac{\pi t}{T_b}\right)=\left(s_{0I}(t)-s_{1I}(t)\right)\sin\frac{\pi t}{T_b} \tag{41b}$$

An example of a set of signals that satisfies the symmetric PSD conditions of Eq. (40) [or Eq. (41)] as well as the foregoing conditions for finite (2-bit) decoding delay and $d^2_{\min}=2$ is given as follows. Analogously to the MSK design of Eq. (16), let

$$\left.\begin{aligned} s_2(t) &= \sin\frac{\pi t}{T_b}-j\cos\frac{\pi t}{T_b} \\ s_0(t) &= 0+j1 \end{aligned}\right\} \tag{42}$$

which clearly satisfies Eq. (40b). Next let

$$s_{1R}(t)+s_{2R}(t)=g_0(t)\cos\frac{\pi t}{2T_b} \tag{43}$$

where $g_0(t)$ is as yet an arbitrary function to be specified. From Eq. (41a), we have

$$s_{1I}(t)+s_{2I}(t)=g_0(t)\cos\frac{\pi t}{2T_b}\left(\frac{1-\cos\frac{\pi t}{T_b}}{\sin\frac{\pi t}{T_b}}\right)=g_0(t)\sin\frac{\pi t}{2T_b} \tag{44}$$

Since, from Eq. (42), $s_{2R}(t)=\sin(\pi t/T_b)$ and $s_{2I}(t)=-\cos(\pi t/T_b)$, then making use of these in Eqs. (43) and (44) gives

$$s_{1R}(t)=g_0(t)\cos\frac{\pi t}{2T_b}-\sin\frac{\pi t}{T_b} \tag{45a}$$

$$s_{1I}(t)=g_0(t)\sin\frac{\pi t}{2T_b}+\cos\frac{\pi t}{T_b} \tag{45b}$$

or

$$s_1(t)=g_0(t)\cos\frac{\pi t}{2T_b}-\sin\frac{\pi t}{T_b}+j\left(g_0(t)\sin\frac{\pi t}{2T_b}+\cos\frac{\pi t}{T_b}\right) \tag{46}$$

Note that, with the above choice of $s_1(t)$ and $s_0(t)$, the relation in Eq. (40c) [or equivalently Eq. (41b)] is automatically satisfied as previously mentioned. The remainder of the signaling set is determined from

$$\left.\begin{aligned} s_3(t) &= s_2(t)-s_0(t)+s_1(t) \\ s_i(t) &= -s_{7-i}(t), \quad i=4,5,6,7 \end{aligned}\right\} \tag{47}$$

The function $g_0(t)$ in Eq. (46) must be chosen to satisfy the unit power condition on the signals, i.e., $(1/T_b)\int_0^{T_b}|s_i(t)|^2\,dt = 1$. Substituting Eq. (46) into this condition and simplifying results in the requirement on $g_0(t)$:

$$\frac{1}{T_b}\int_0^{T_b} g_0^2(t)\,dt = \frac{2}{T_b}\int_0^{T_b} g_0(t)\sin\frac{\pi t}{2T_b}dt \tag{48}$$

It can also be shown that the condition of Eq. (48) results in $(1/T_b)\int_0^{T_b}|s_3(t)|^2\,dt = 1$, which completes the unit power requirement on the entire signal set.

Clearly, the function $g_0(t) = 2\sin\pi t/2T_b$ will satisfy Eq. (48). However, this results in redundant signals since now [see Eqs. (43) and (39)] $s_1(t)$ becomes equal to $s_0(t)$ and also $s_3(t)$ becomes equal to $s_2(t)$, which furthermore produces a memory-two PSD equal to that of memory-one MSK, i.e., no improvement. Thus, we must perturb $g_0(t)$ away from $2\sin\pi t/2T_b$ to obtain a distinct signal set. What remains is to determine suitable choices for $g_0(t)$ that yield improved (relative to MSK-type memory-one schemes) bandwidth efficiency.

Before doing so, however, we first extend the above considerations to generalized MSK. If instead of Eq. (42) we were to choose the signals corresponding to Eq. (34), i.e.,

$$\left.\begin{aligned} s_0(t) &= \sin\left(\pi\left(f(t)-\frac{t}{2T_b}\right)\right) + j\cos\left(\pi\left(f(t)-\frac{t}{2T_b}\right)\right)\\ s_2(t) &= \sin\left(\pi\left(f(t)+\frac{t}{2T_b}\right)\right) - j\cos\left(\pi\left(f(t)+\frac{t}{2T_b}\right)\right)\end{aligned}\right\} \tag{49}$$

then the replacement for Eq. (46) would become

$$s_1(t) = g_0(t)\cos\frac{\pi t}{2T_b} - \sin\left(\pi\left(f(t)+\frac{t}{2T_b}\right)\right) + j\left[g_0(t)\sin\frac{\pi t}{2T_b} + \cos\left(\pi\left(f(t)+\frac{t}{2T_b}\right)\right)\right] \tag{50}$$

Applying the unit power condition to Eq. (50) results in the requirement on $g_0(t)$, analogous to Eq. (48),

$$\frac{1}{T_b}\int_0^{T_b} g_0^2(t)\,dt = \frac{2}{T_b}\int_0^{T_b} g_0(t)\sin\pi f(t)\,dt \tag{51}$$

Finally, starting with the optimum memory-one solution, namely, the particular $s_0(t)$ and $s_1(t)$ that satisfy Eq. (28) and also achieve the best bandwidth efficiency (to be discussed in the next section), we can arrive at an optimum memory-two solution as follows. Let $s_0^{(1)}(t)$ and $s_1^{(1)}(t)$ denote this optimum memory-one solution. Then, since for memory two the condition of Eq. (40b) is analogous to Eq. (28), we choose

$$\left.\begin{aligned} s_0^{(2)}(t) &\triangleq s_{0R}^{(2)}(t) + j s_{0I}^{(2)}(t) = s_0^{(1)}(t)\\ s_2^{(2)}(t) &\triangleq s_{2R}^{(2)}(t) + j s_{2I}^{(2)}(t) = s_1^{(1)}(t)\end{aligned}\right\} \tag{52}$$

and from Eqs. (43) and (5a),

$$\left.\begin{aligned} s_1^{(2)}(t) &= g_0(t)\cos\frac{\pi t}{2T_b} - s_{2R}^{(2)}(t) + j\left(g_0(t)\sin\frac{\pi t}{2T_b} - s_{2I}^{(2)}(t)\right) \\ s_3^{(2)}(t) &= s_2^{(2)}(t) - s_0^{(2)}(t) + s_1^{(2)}(t) \end{aligned}\right\} \tag{53}$$

where, from the unit power condition applied to $s_1^{(2)}(t)$, $g_0(t)$ must satisfy[7]

$$\begin{aligned} \frac{1}{T_b}\int_0^{T_b} g_0^2(t)\,dt &= \frac{2}{T_b}\int_0^{T_b} g_0(t)\left[s_{2R}^{(2)}(t)\cos\frac{\pi t}{2T_b} + s_{2I}^{(2)}(t)\sin\frac{\pi t}{2T_b}\right]dt \\ &= \frac{2}{T_b}\int_0^{T_b} g_0(t)\left[s_{1R}^{(1)}(t)\cos\frac{\pi t}{2T_b} + s_{1I}^{(1)}(t)\sin\frac{\pi t}{2T_b}\right]dt \end{aligned} \tag{54}$$

Although as previously stated $g_0(t)$ is as yet arbitrary, it must be scaled so as to satisfy Eq. (54). To determine this scale factor, we write $g_0(t)$ as $g_0(t) = KG_0(t)$, whereupon substitution in Eq. (54) gives the solution for K as

$$K = \frac{\frac{2}{T_b}\int_0^{T_b} G_0(t)\left[s_{1R}^{(1)}(t)\cos\frac{\pi t}{2T_b} + s_{1I}^{(1)}(t)\sin\frac{\pi t}{2T_b}\right]dt}{\frac{1}{T_b}\int_0^{T_b} G_0^2(t)dt} \tag{55}$$

Thus, Eqs. (52) through (55) represent *a formal procedure for designing an optimum memory-two signal set entirely in terms of the optimum memory-one solution* $s_0^{(1)}(t) = s_{0R}^{(1)}(t) + js_{0I}^{(1)}(t)$.[8]

Following along the lines of Eqs. (29) and (30), the equivalent PSD of the memory-two modulation may be found. In particular, the Fourier transform of the equivalent pulse shape in Eq. (8) is given as

$$P(f) = \frac{1}{2}\left[S_0(f) + S_3(f) + e^{-j2\pi fT_b}\big(S_0(f) - S_2(f)\big) + e^{-j4\pi fT_b}\big(S_0(f) - S_1(f)\big)\right] \tag{56}$$

Using the additional relation $S_3(f) = S_1(f) + S_2(f) - S_0(f)$ to achieve finite decoding delay, one immediately gets

---

[7] Note that the condition of Eq. (54) also results in $(1/T_b)\int_0^{T_b}|s_3(t)|^2dt = 1$, as required.

[8] This statement can be generalized to apply to arbitrary memory ν. In particular, it can be shown that an optimum solution for memory ν can be obtained by using the optimum solution for memory $\nu - 1$ as a subset of the signal design, with the remainder of signals obtained from the signal difference conditions of Eqs. (6) and (7) and the design of only one additional signal based upon a procedure analogous to Eqs. (52) through (55). Finally, we point out that the foregoing procedure represents a sufficient (but not necessary) condition for arriving at an optimum solution.

$$\frac{1}{T_b}\left|P\left(f\right)\right|^2 = \frac{1}{4T_b}\Big[\left|S_1\left(f\right)+S_2\left(f\right)\right|^2 + \left|S_0\left(f\right)-S_2\left(f\right)\right|^2 + \left|S_0\left(f\right)-S_1\left(f\right)\right|^2$$
$$+2\ \mathrm{Re}\left\{\left(S_1^*\left(f\right)+S_2^*\left(f\right)\right)\left(S_0\left(f\right)-S_2\left(f\right)\right)e^{-j2\pi fT_b}\right\}$$
$$+2\ \mathrm{Re}\left\{\left(S_0^*\left(f\right)-S_2^*\left(f\right)\right)\left(S_0\left(f\right)-S_1\left(f\right)\right)e^{-j2\pi fT_b}\right\}$$
$$+2\ \mathrm{Re}\left\{\left(S_1^*\left(f\right)+S_2^*\left(f\right)\right)\left(S_0\left(f\right)-S_1\left(f\right)\right)e^{-j4\pi fT_b}\right\}\Big] \tag{57}$$

Finally, the desired equivalent lowpass PSD is

$$\frac{1}{T_b}\left|P\left(f+\frac{1}{4T_b}\right)\right|^2 = \frac{1}{4T_b}\Bigg[\left|S_1\left(f+\frac{1}{4T_b}\right)+S_2\left(f+\frac{1}{4T_b}\right)\right|^2$$
$$+\left|S_0\left(f+\frac{1}{4T_b}\right)-S_2\left(f+\frac{1}{4T_b}\right)\right|^2+\left|S_0\left(f+\frac{1}{4T_b}\right)-S_1\left(f+\frac{1}{4T_b}\right)\right|^2$$
$$+2\,\mathrm{Re}\left\{\left(S_1^*\left(f+\frac{1}{4T_b}\right)+S_2^*\left(f+\frac{1}{4T_b}\right)\right)\left(S_0\left(f+\frac{1}{4T_b}\right)-S_2\left(f+\frac{1}{4T_b}\right)\right)e^{-j2\pi[f+(1/4T_b)]T_b}\right\}$$
$$+2\,\mathrm{Re}\left\{\left(S_0^*\left(f+\frac{1}{4T_b}\right)-S_2^*\left(f+\frac{1}{4T_b}\right)\right)\left(S_0\left(f+\frac{1}{4T_b}\right)-S_1\left(f+\frac{1}{4T_b}\right)\right)e^{-2\pi[f+(1/4T_b)]T_b}\right\}$$
$$+2\,\mathrm{Re}\left\{\left(S_1^*\left(f+\frac{1}{4T_b}\right)+S_2^*\left(f+\frac{1}{4T_b}\right)\right)\left(S_0\left(f+\frac{1}{4T_b}\right)-S_1\left(f+\frac{1}{4T_b}\right)\right)e^{-4\pi[f+(1/4T_b)]T_b}\right\}\Bigg] \tag{58}$$

Since the symmetry conditions in Eq. (39) result in

$$\left.\begin{aligned}
S_1\left(f+\frac{1}{4T_b}\right)+S_2\left(f+\frac{1}{4T_b}\right) &= S_1^*\left(-f+\frac{1}{4T_b}\right)+S_2^*\left(-f+\frac{1}{4T_b}\right)\\
S_0\left(f+\frac{1}{4T_b}\right)-S_2\left(f+\frac{1}{4T_b}\right) &= S_0^*\left(-f+\frac{1}{4T_b}\right)-S_2^*\left(-f+\frac{1}{4T_b}\right)\\
S_0\left(f+\frac{1}{4T_b}\right)-S_1\left(f+\frac{1}{4T_b}\right) &= S_0^*\left(-f+\frac{1}{4T_b}\right)-S_1^*\left(-f+\frac{1}{4T_b}\right)
\end{aligned}\right\} \tag{59}$$

then Eq. (58) is clearly an even function of frequency.

IV. Optimizing the Bandwidth Efficiency

Having now obtained expressions for the equivalent baseband PSD, it is now straightforward to use these to determine the sets of signals that satisfy all of the previous constraints and in addition maximize the power within a given bandwidth, B. In mathematical terms, we search for the set of signals that for a given value of B maximizes the fractional in-band power

$$\left.\begin{aligned} \eta &= \frac{\int_{-B/2}^{B/2} G(f)df}{\int_{-\infty}^{\infty} G(f)df} \\ G(f) &\triangleq \frac{1}{T_b}\left|P\left(f+\frac{1}{4T_b}\right)\right|^2 \end{aligned}\right\} \tag{60}$$

subject to the unit power constraint

$$\frac{1}{T_b}\int_0^{T_b}\left|s_i(t)\right|^2 dt = 1, \quad i = 0, 1, 2, \cdots, M-1 \tag{61}$$

A. Memory-One Case

For the case of $\nu = 1$, we observed that the entire signal set may be determined from the single complex signal $s_0(t)$. Thus, the optimization of bandwidth efficiency corresponds to substituting the PSD of Eq. (31) [which is entirely specified in terms of the Fourier transform of $s_0(t)$] into Eq. (60) and then maximizing η subject to Eq. (61) or equivalently from Parseval's theorem

$$\frac{1}{T_b}\int_{-\infty}^{\infty}\left|S_0(f)\right|^2 dt = 1 \tag{62}$$

Such a procedure would result in an optimum $S_0(f)$ from whose inverse Fourier transform one could determine the optimum signal set. Since $S_0(f)$ exists, in general, over the entire doubly infinite frequency axis, it is perhaps simpler to approach the optimization in the time domain since $s_0(t)$ is indeed time limited to the interval $0 \le t \le T_b$. To do this, we first need to rewrite the PSD of Eq. (31) in terms of $s_0(t)$ rather than $S_0(f)$ and then to perform the integrations on f required in Eq. (60). After considerable manipulation, and for simplicity of notation normalizing $T_b = 1$ (i.e., $BT_b = B$), it can be shown that

$$\begin{aligned} &\int_{-B/2}^{B/2} G(f)\,df = \\ &\quad B\int_0^1\int_0^1 s_0(t)\,s_0^*(\tau)\,e^{-j(\pi/2)(t-\tau)}\left[\operatorname{sinc}\pi B(t-\tau) - j\frac{1}{2}\operatorname{sinc}\pi B(t-\tau+1)\right. \\ &\quad \left. +j\frac{1}{2}\operatorname{sinc}\pi B(t-\tau-1)\right]dtd\tau \\ &\quad +\frac{1}{2}B\ \operatorname{Im}\left\{\int_0^1\int_0^1 s_0(t)\,s_0(\tau)\,e^{-j(\pi/2)(t+\tau)}\left[\operatorname{sinc}\pi B(t-\tau+1)+\operatorname{sinc}\pi B(t-\tau-1)\right]dtd\tau\right\} \end{aligned} \tag{63}$$

where $\operatorname{sinc} x \triangleq \sin x/x$. Furthermore, it is straightforward to show that

$$\int_{-\infty}^{\infty} G(f)\, df = 1 \tag{64}$$

and thus η is given by Eq. (63).

As a check on Eq. (63), consider its evaluation for the MSK signal of Eq. (16). Substituting $s_0(t) = 0 + j1$ in Eq. (63) and simplifying gives

$$\begin{aligned}
\int_{-B/2}^{B/2} G(f)\, df &= B \int_0^1 \int_0^1 \cos\frac{\pi}{2}(t-\tau)\, \operatorname{sinc} \pi B(t-\tau)\, dt d\tau \\
&\quad + B \int_0^1 \int_0^1 \sin\frac{\pi}{2} t \cos\frac{\pi}{2}\tau \operatorname{sinc} \pi B(t-\tau-1)\, dt d\tau \\
&\quad + B \int_0^1 \int_0^1 \cos\frac{\pi}{2} t \sin\frac{\pi}{2}\tau \operatorname{sinc} \pi B(t-\tau+1)\, dt d\tau \\
&= B \int_0^1 \int_0^1 \cos\frac{\pi}{2}(t-\tau)\, \operatorname{sinc} \pi B(t-\tau)\, dt d\tau \\
&\quad + 2B \int_0^1 \int_0^1 \sin\frac{\pi}{2} t \cos\frac{\pi}{2}\tau \operatorname{sinc} \pi B(t-\tau-1)\, dt d\tau
\end{aligned} \tag{65}$$

The conventional computation of the PSD of MSK is obtained from

$$G(f) = \frac{1}{2T_b}\left|\mathcal{F}\left\{\sqrt{2}\sin\frac{\pi t}{2T_b}\right\}\right|^2 = \left|\mathcal{F}\left\{\sin\frac{\pi t}{2}\right\}\right|^2 = \left|\int_0^2 \sin\frac{\pi t}{2} e^{-j2\pi f t} dt\right|^2 = \frac{16}{\pi^2}\frac{\cos^2 2\pi f}{(1-16f^2)^2} \tag{66}$$

where the latter equalities assume $T_b = 1$. Partitioning the integral in Eq. (66) into two integrals corresponding to the adjacent time intervals $0 \le t \le 1$ and $1 \le t \le 2$, then making a change of variables in the second integral to shift it to the interval $0 \le t \le 1$, and finally integrating the result on f between the limits $-B/2$ and $B/2$ produces the identical result to that of Eq. (65).

The maximization of Eq. (63) subject to the energy constraint of Eq. (61) has been carried out numerically using the MATLAB$^{(R)}$ optimization toolbox function "fminunc" (quasi-Newton method of convergence). In particular, for each value of B (BT_b if $T_b \neq 1$), the optimum complex signal $s_0(t)$ (represented by N uniformly spaced samples in the interval $(0, 1)$) is determined from which the fractional

out-of-band power $1-\eta$ is calculated using Eq. (63) for η. Because of complexity issues involved in computing the optimum solution, the number of sample points N is limited to 64. Furthermore, since the Gaussian integration required to evaluate the double integral of Eq. (63) requires a much higher density of sample values (not necessarily uniformly spaced), and to allow for Fourier interpolation, we assume the signal to be bandlimited[9] to the Nyquist rate, i.e., 32 ($32/T_b$ if $T_b \neq 1$). Because of this bandlimiting assumption, certain optimum signal waveforms (particularly those at small values of B) that exhibit a sharp discontinuity will have a ringing behavior. This ringing behavior can be minimized by additional interpolation (filtering) but has proven difficult to eliminate completely.

Figures 4(a) and 4(b) are 3-D plots of the optimum real and imaginary parts of $s_0(t)$ versus t as a function of B (or equivalently, BT_b with $T_b = 1$) in the interval $0 \leq B \leq 3$. Figures 5(a) through 5(h) are a number of cuts of these 3-D plots taken at distinct values of B in the same range. For small values of B, we observe that the real part of $s_0(t)$ has sharp discontinuities at $t = 0$ and $t = 1$ and thus exhibits the ringing behavior alluded to above. As B increases, the sharpness of the discontinuity at the edges diminishes, and in the limit of large B, both the real and imaginary parts of $s_0(t)$ approach a sinusoidal behavior with unit period. Specifically, $s_0(t)$ tends toward the form $-\alpha_1 \sin 2\pi t + j(\beta_1 + \alpha_2 \cos 2\pi t)$, where α_1, α_2, and β_1 are constants that also must satisfy the unit energy constraint of Eq. (60), i.e., $\beta_1^2 + (1/2)\left(\alpha_1^2 + \alpha_2^2\right) = 1$. Figure 6 is the corresponding plot of optimum (minimum) fractional out-of-band power versus B. Also shown are corresponding results for MSK and SFSK modulations, which can readily be found in [4, Fig. 2.11]. We observe that by optimizing the signal set at each value of B without loss in $d_{\min}^2$ or finite decoding delay performance, we are able to obtain a significant improvement in bandwidth efficiency. The quantitative amount of this improvement is given in Table 1 for the 99 percent and 99.9 percent bandwidths corresponding respectively to the -20 dB and -30 dB out-of-band power levels.

Before concluding this section, we note that the maximization of Eq. (63) subject to the constraint in Eq. (62) can be carried out analytically using the method of calculus of variations. Unfortunately, however, the resulting solution for $s_0(t)$ is in the form of an integral equation that does not lend itself to a closed-form solution. Thus, there is no strong advantage to presenting these results here since we have already obtained a numerical solution as discussed above by direct maximization of Eq. (63). One interesting observation does result from applying the calculus of variations approach and this is that $s_{0R}(t)$ is an odd function around its midpoint (at $t = 1/2$) and $s_{0I}(t)$ is an even function around its same midpoint. Clearly, this observation is justified by the numerical results illustrated in the various parts of Fig. 5.

B. Memory-Two Case

Analogous to what was done for the memory-one case, we need to maximize the fractional in-band power of Eq. (60) using now Eq. (58) for $G(f)$. Expressing the various Fourier transforms of Eq. (58) in terms of their associated signal waveforms and then performing the integration on frequency between $-B/2$ and $B/2$ as required in Eq. (60) produces the following result (again normalizing $T_b = 1$):

$$\int_{-B/2}^{B/2} G(f)\, df = \sum_{i=1}^{6} P_i \tag{67}$$

where

[9] Of course, in reality the continuous time-limited signal $s_0(t)$ would have infinite bandwidth.

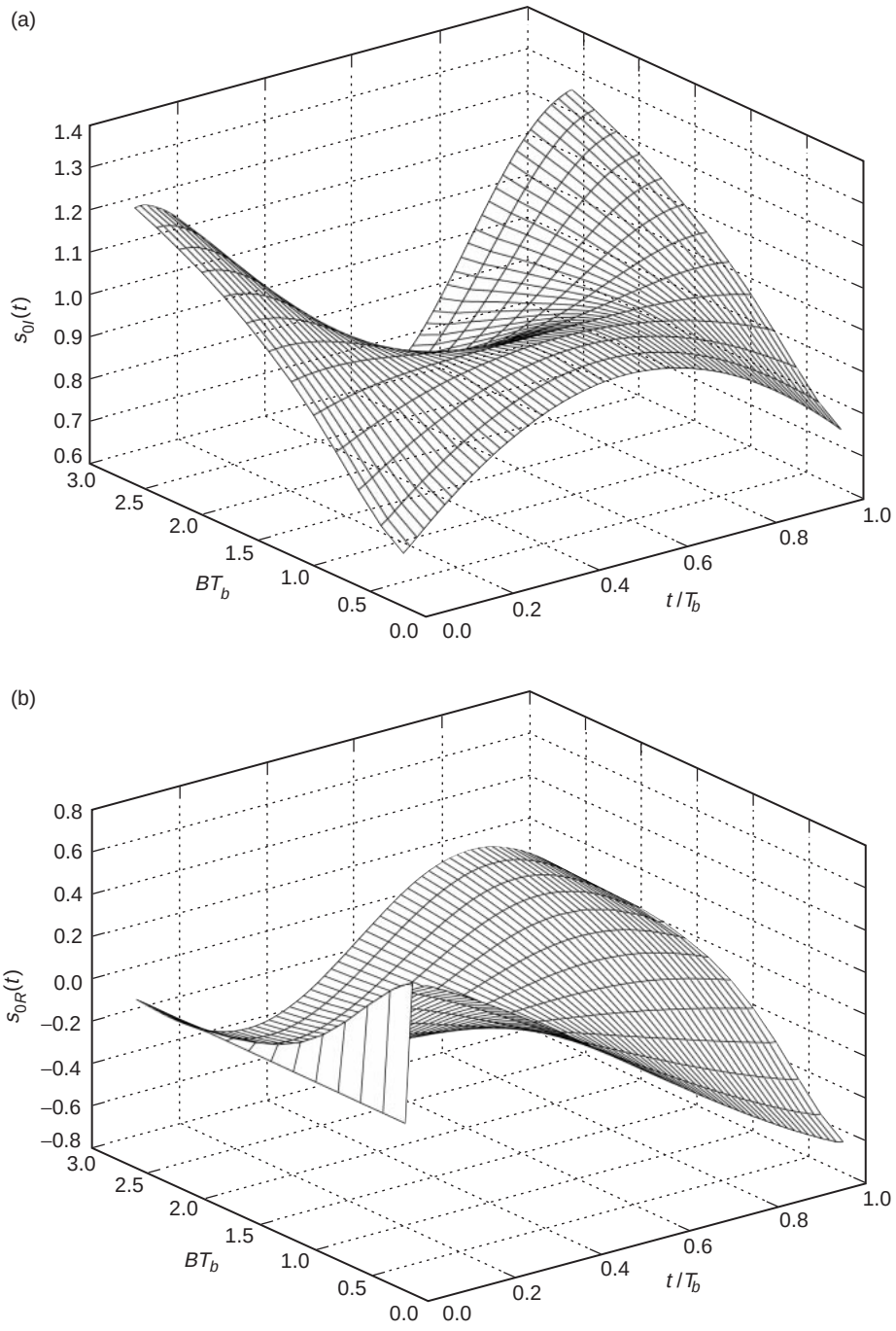

Fig. 4. Profiles of the optimum signal as a function of the bandwidth–bit time product: (a) the imaginary part and (b) the real part.

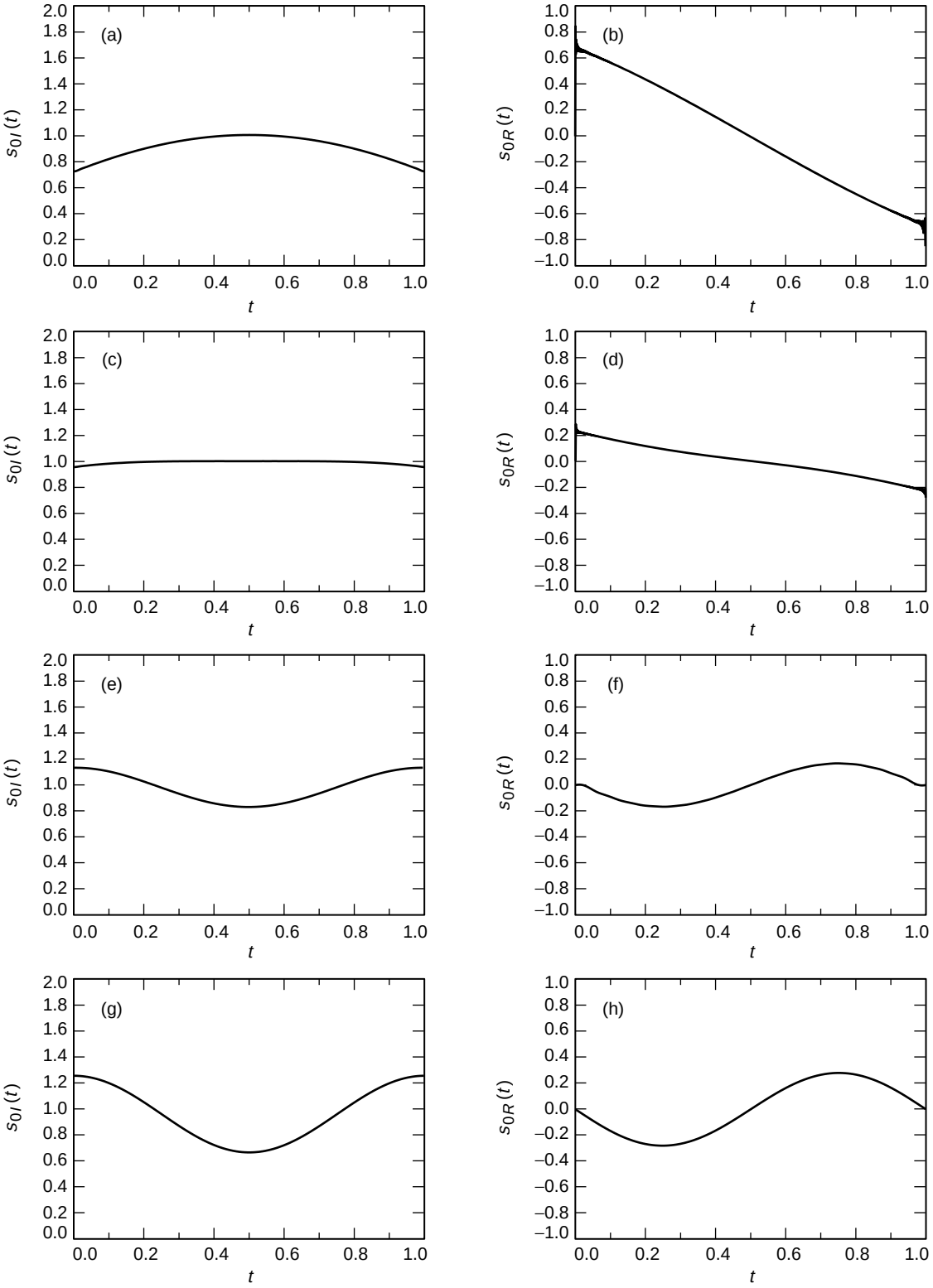

Fig. 5. Real and imaginary parts of the optimum signal for the given bandwidth–time product: (a) imaginary part, BT_b = 0.2, (b) real part, BT_b = 0.2, (c) imaginary part, BT_b = 1.0, (d) real part, BT_b = 1.0, (e) imaginary part, BT_b = 1.8, (f) real part, BT_b = 1.8, (g) imaginary part, BT_b = 2.6, and (h) real part, BT_b = 2.6.

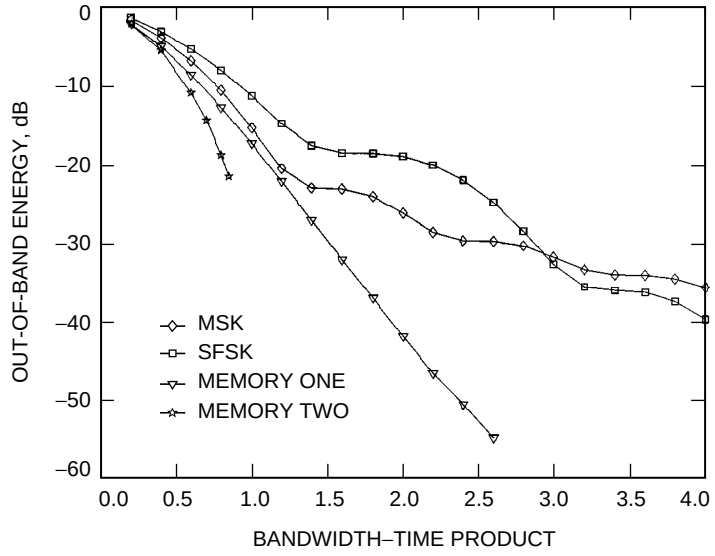

Fig. 6. Comparison of fractional out-of-band energies.

$$P_1 = \frac{B}{4}\int_0^1\int_0^1 \left(s_1^{(2)}(t)+s_2^{(2)}(t)\right)\left(s_1^{(2)}(\tau)+s_2^{(2)}(\tau)\right)^* e^{-j(\pi/2)(t-\tau)}\operatorname{sinc}\pi B(t-\tau)\,dtd\tau$$

$$P_2 = \frac{B}{4}\int_0^1\int_0^1 \left(s_0^{(2)}(t)-s_2^{(2)}(t)\right)\left(s_0^{(2)}(\tau)-s_2^{(2)}(\tau)\right)^* e^{-j(\pi/2)(t-\tau)}\operatorname{sinc}\pi B(t-\tau)\,dtd\tau$$

$$P_3 = \frac{B}{4}\int_0^1\int_0^1 \left(s_0^{(2)}(t)-s_1^{(2)}(t)\right)\left(s_0^{(2)}(\tau)-s_1^{(2)}(\tau)\right)^* e^{-j(\pi/2)(t-\tau)}\operatorname{sinc}\pi B(t-\tau)\,dtd\tau$$

$$P_4 = 2\,\mathrm{Re}\left\{\frac{B}{4}\int_0^1\int_0^1 \left(s_0^{(2)}(t)-s_2^{(2)}(t)\right)\left(s_1^{(2)}(\tau)+s_2^{(2)}(\tau)\right)^* e^{-j(\pi/2)(t-\tau+1)}\operatorname{sinc}\pi B(t-\tau+1)\,dtd\tau\right\}$$

$$P_5 = 2\,\mathrm{Re}\left\{\frac{B}{4}\int_0^1\int_0^1 \left(s_0^{(2)}(t)-s_1^{(2)}(t)\right)\left(s_0^{(2)}(\tau)-s_2^{(2)}(\tau)\right)^* e^{-j(\pi/2)(t-\tau+1)}\operatorname{sinc}\pi B(t-\tau+1)\,dtd\tau\right\}$$

$$P_6 = 2\,\mathrm{Re}\left\{\frac{B}{4}\int_0^1\int_0^1 \left(s_0^{(2)}(t)-s_1^{(2)}(t)\right)\left(s_1^{(2)}(\tau)+s_2^{(2)}(\tau)\right)^* e^{-j(\pi/2)(t-\tau+2)}\operatorname{sinc}\pi B(t-\tau+2)\,dtd\tau\right\} \tag{68}$$

Since, for a given B, $s_0^{(2)}(t)$ and $s_2^{(2)}(t)$ are considered known by virtue of the memory-one solution [see Eq. (52)], then $s_1^{(2)}(t)$ is the only signal waveform that needs to be determined by maximization of Eq. (60) combined with Eq. (68). (Note that $s_3^{(2)}(t)$ can be found from the second relation in Eq. (53) once $s_1^{(2)}(t)$ is determined.) Also, since the term P_2 in Eq. (68) does not depend on $s_1^{(2)}(t)$, it can be omitted from the maximization.

Table 1. Bandwidth-efficient performance of TCM with prescribed decoding delay.

Signal	$1/B_{99}T_b$, (b/s)/Hz	Improvement over MSK, percent	$1/B_{99.9}T_b$, (b/s)/Hz	Improvement over MSK, percent
MSK	0.845	—	0.366	—
Optimum ($\nu = 1$)	0.896	6.04	0.659	79.7
Optimum ($\nu = 2$)	1.23	45.6	—	—

V. Bandwidth-Efficient TCM with Prescribed Decoding Delay and Unequal Energy Signals

In the introduction, we alluded to the fact that a relaxation of the equal-energy condition on the signals potentially could be used to trade off between the power and bandwidth efficiency of the system. We now investigate the additional constraints that must be placed on the signals in order for the optimum TCM receiver to still achieve a finite decoding delay equal to the memory of the modulation. In order to accomplish this, we first briefly review the received signal-plus-noise model, branch metric, and accompanying decision rule leading up to the conditions on the signal differences in Theorem I of [1] [summarized herein in Eqs. (6) and (7)] and then modify them so as to apply to the case of unequal signal energies.

Corresponding to the baseband signal $s(t)$ of Eq. (1) transmitted over an additive white Gaussian noise (AWGN) channel, the received signal is

$$R(t) = s(t) + N(t) \tag{69}$$

where $N(t)$ is a zero-mean complex Gaussian noise process with PSD N_0 W/Hz. For equal energy signals, the maximum-likelihood (Viterbi) receiver uses as its branch metric in the nth interval

$$\lambda_n(s_i) = \mathrm{Re}\left\{\int_{nT}^{(n+1)T} R^*(t)\, s_i(t - nT)\, dt\right\}$$

$$= \mathrm{Re}\left\{\int_0^T R^*(t + nT)\, s_i(t)\, dt\right\}, \quad i \in \left\{0, 1, \cdots, 2^{\nu+1} - 1\right\} \tag{70}$$

Without any constraints on the signal set, for true optimality the Viterbi receiver *theoretically* needs to observe the entire transmitted sequence (sum over an infinite number of branch metrics), resulting in an infinite decoding delay, although in practice one may decode with finite delay using a truncated (but suboptimal) form of Viterbi algorithm [7]. If the signal differences are constrained as in Eqs. (6) and (7), then, as previously stated in Theorem I of [1], the receiver can optimally decode the nth information symbol after ν symbol intervals according to the decision rule:

$$\text{choose } U_n = 0 \text{ if } \sum_{i=\nu}^{n+\nu} \lambda_i\left(s_0 - s_{2^{n+\nu-i}}\right) > 0, \quad \text{otherwise choose } U_n = 1 \tag{71}$$

For unequal energy signals, the branch metric of Eq. (70) would be modified to

$$\lambda_n(s_i) = \mathrm{Re}\left\{\int_{nT}^{(n+1)T} R^*(t)\, s_i(t-nT)\, dt\right\} - \frac{E_i}{2}$$

$$= \mathrm{Re}\left\{\int_0^T R^*(t+nT)\, s_i(t)\, dt\right\} - \frac{E_i}{2}, \quad i \in \left\{0, 1, \cdots, 2^{\nu+1}-1\right\} \tag{72}$$

where $E_i = \int_0^T |s_i(t)|^2\, dt$ is the energy of the ith signal in the set. Since the derivation of the conditions for finite decoding delay given in [1] relies on comparisons of sums of branch metrics, it is straightforward to substitute Eq. (72) for Eq. (70) in the steps of this derivation, which leads to an additional set of conditions on the energies of the signals. To illustrate the procedure, we first consider the simplest case corresponding to unit memory ($\nu = 1$).

Consider the two-state trellis (corresponding to the nth and $n+1$st intervals) in Fig. 7, where each branch is labeled with (1) the input bit that causes the transition between states and (2) the baseband signal transmitted in accordance with the choice defined in Fig. 1(b). Assume first that we are in state "0" at time n (having gotten there as a result of decoding symbols in the previous intervals). Suppose now that the two paths (of length-two branches) that survive at time $n+2$ are those that merge at (emanate from) the same node at time $n+1$ (thereby allowing unique decoding of the transmitted symbol U_n). Since this node can correspond to either state "0" or state "1," there exist two possibilities, which are indicated by heavy lines in Figs. 7(a) and 7(b).

For Fig. 7(a), both surviving paths have a first branch corresponding to $U_n = 1$ and thus the decision $\hat{U}_n = 1$ is unique provided that

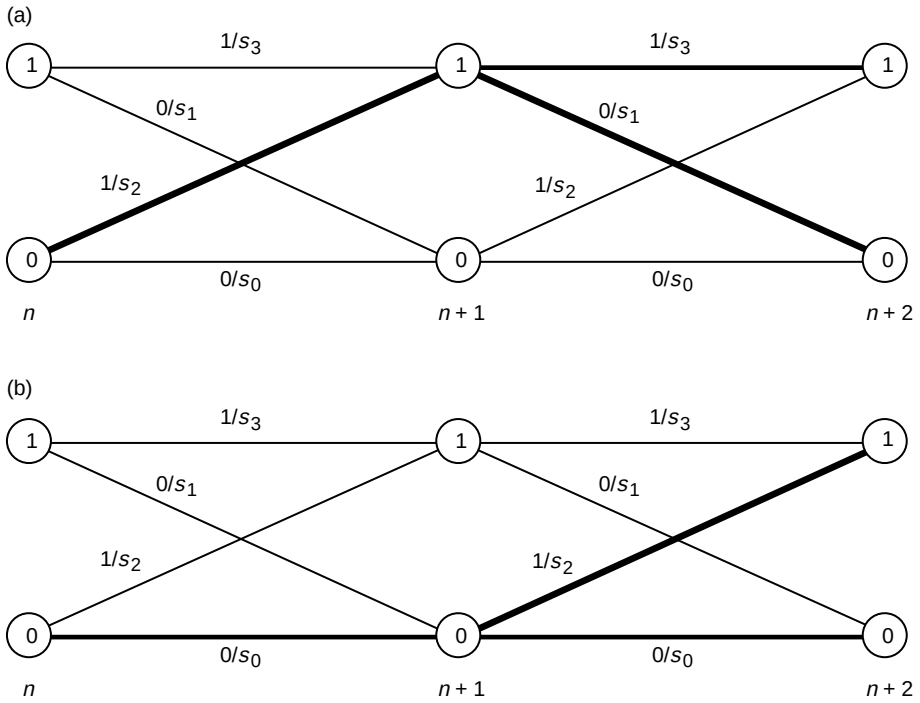

Fig. 7. Trellis diagram for memory-one modulation assuming state "0" at time *n*: (a) surviving paths merging at state "1" at time *n* + 1 and (b) surviving paths merging at state "0" at time *n* + 1.

$$\lambda_n(s_2) + \lambda_{n+1}(s_3) > \lambda_n(s_0) + \lambda_{n+1}(s_2) \tag{73a}$$

and

$$\lambda_n(s_2) + \lambda_{n+1}(s_1) > \lambda_n(s_0) + \lambda_{n+1}(s_0) \tag{73b}$$

or, equivalently,

$$\lambda_n(s_0) - \lambda_n(s_2) + \lambda_{n+1}(s_2) - \lambda_{n+1}(s_3) < 0 \tag{74a}$$

and

$$\lambda_n(s_0) - \lambda_n(s_2) + \lambda_{n+1}(s_0) - \lambda_{n+1}(s_1) < 0 \tag{74b}$$

To simultaneously satisfy Eqs. (74a) and (74b), we need to have

$$\lambda_{n+1}(s_2) - \lambda_{n+1}(s_3) = \lambda_{n+1}(s_0) - \lambda_{n+1}(s_1) \tag{75}$$

which is the identical requirement found by Li and Rimoldi [1] when treating the equal signal energy case. Now using instead the metric definition in Eq. (71) for unequal energy signals, then, analogously to the results in [1], the condition of Eq. (75) can be satisfied by the first equality in Eq. (5a), namely,

$$s_0(t) - s_1(t) = s_2(t) - s_3(t) \tag{76}$$

and in addition

$$E_0 - E_1 = E_2 - E_3 \tag{77}$$

Note that the relation in Eq. (77) is identical in form to that in Eq. (76) if each of the signals in the latter is replaced by its energy. This observation will carry over when considering modulations with memory greater than one.

For Fig. 7(b), both surviving paths have a first branch corresponding to $U_n = 0$ and thus the decision $\hat{U}_n = 0$ is unique provided that

$$\lambda_n(s_0) + \lambda_{n+1}(s_2) > \lambda_n(s_2) + \lambda_{n+1}(s_3) \tag{78a}$$

and

$$\lambda_n(s_0) + \lambda_{n+1}(s_0) > \lambda_n(s_2) + \lambda_{n+1}(s_1) \tag{78b}$$

or, equivalently,

$$\lambda_n(s_0) - \lambda_n(s_2) + \lambda_{n+1}(s_2) - \lambda_{n+1}(s_3) > 0 \tag{79a}$$

and

$$\lambda_n(s_0) - \lambda_n(s_2) + \lambda_{n+1}(s_0) - \lambda_{n+1}(s_1) > 0 \tag{79b}$$

It is clear that the condition in Eq. (75) will also simultaneously satisfy Eqs. (79a) and (79b).

Finally, had we assumed that we were in state "1" at time n, then it would be straightforward to show that the conditions on the signal set that produce a unique decision on U_n would be identical to those in Eqs. (76) and (77). Thus, we conclude that, *for a memory-one modulation of the type described by Fig. 1(b) with unequal energy signals, the conditions on the signal set to guarantee unique decodability with 1-symbol delay are those given in Eqs. (76) and (77).*

To extend the above to modulations with memory ν greater than one, we proceed as follows. As was observed in [1], what we now seek are the inequality conditions on the sums of branch metrics such that the 2^ν surviving paths at time $n+\nu$ merge at a single node at time $n+1$. Given a particular state at time n, this set of 2^ν conditions then allows for uniquely decoding U_n. Since these conditions are expressed entirely in terms of the branch metrics for the surviving paths and as such do not depend on the form of the metric itself (i.e., whether it be Eq. (69) for equal energy signals or Eq. (71) for unequal energy signals), then it is straightforward to conclude that the finite decoding delay conditions on the signal set derived in [1] for the equal-energy case also apply now to the signal energies in the nonequal-energy case. Specifically, in addition to Eq. (6), the signal set must satisfy the energy conditions

$$E_0 - E_{2^m} = E_{2^{m+1}l} - E_{2^{m+1}l+2^m}, \quad m = 0, 1, 2, \cdots, \nu - 1, \quad l = 1, 2, \cdots, 2^{\nu-m} - 1 \tag{80}$$

Clearly, for the equal-energy case, Eq. (80) is trivially satisfied.

Having now specified the conditions for achieving finite decoding delay with unequal energy signals, we now investigate the impact of this relaxed restriction on the minimum-squared Euclidean distance (power efficiency) of the modulation. Again, consider first the memory-one case. For the trellis diagram of Fig. 7(a), the unnormalized squared Euclidean distance between the length-two error event path and the all-zeros path (corresponding to $U_n = 0, U_{n+1} = 0$) is

$$\begin{aligned} D^2 &= \int_0^T \left|s_0(t) - s_2(t)\right|^2 dt + \int_0^T \left|s_0(t) - s_1(t)\right|^2 dt \\ &= 2E_0 + E_1 + E_2 - 2\,\mathrm{Re}\left\{\int_0^T s_0^*(t)\left(s_1(t) + s_2(t)\right)dt\right\} \end{aligned} \tag{81}$$

Using Eqs. (76) and (77) in Eq. (81) enables rewriting it in the form

$$\left.\begin{aligned} D^2 &= 2E_{av} - 2\,\mathrm{Re}\left\{\int_0^T s_0^*(t)\, s_3(t)\, dt\right\} \\ E_{av} &= \frac{E_0 + E_1 + E_2 + E_3}{4} = \frac{E_0 + E_3}{2} \end{aligned}\right\} \tag{82}$$

which, when normalized by the average energy of the signal set, E_{av}, gives

$$d^2 \triangleq \frac{D^2}{2E_{av}} = 1 - \frac{\mathrm{Re}\left\{\int_0^T s_0^*(t)\, s_3(t)\, dt\right\}}{E_{av}} = 1 - \frac{\mathrm{Re}\left\{\int_0^T s_0^*(t)\, s_3(t)\, dt\right\}}{(E_0 + E_3)/2} \tag{83}$$

Following steps analogous to Eqs. (81) through (83) and using the signal difference property in Eq. (76), it is straightforward to show that the unnormalized squared Euclidean distance between *any* pair of length-two paths beginning and ending at the same node (i.e., other pairwise error events) is given by Eq. (83), i.e., the trellis has a uniform error probability (UEP) property. It can also be shown, using a combination of Eqs. (76) and (77) in Eq. (81), that Eq. (83) can be expressed as

$$d^2 \triangleq \frac{D^2}{2E_{av}} = 1 - \frac{\mathrm{Re}\left\{\int_0^T s_1^*(t)\, s_2(t)\, dt\right\}}{(E_1 + E_2)/2} \tag{84}$$

Finally, noting that $-1 \leq \mathrm{Re}\left\{\int_0^T s_0^*(t)\, s_3(t)\, dt\right\} / \left[(E_0 + E_3)/2\right]$ with equality achieved when $s_0(t) = -s_3(t)$ and likewise $-1 \leq \mathrm{Re}\left\{\int_0^T s_1^*(t)\, s_2(t)\, dt\right\} / \left[(E_1 + E_2)/2\right]$ with equality achieved when $s_1(t) = -s_2(t)$, then, in order to achieve the maximum value $d^2_{\min} = 2$, we would need to choose $s_0(t) = -s_3(t)$, which produces $E_0 = E_3$ and also $s_1(t) = -s_2(t)$, which produces $E_1 = E_2$. However, from Eq. (77), $E_0 + E_3 = E_1 + E_2$ and thus $E_0 = E_1 = E_2 = E_3 = E$, i.e., all signals have equal energy. Thus, we conclude that, *for memory one, an unequal energy signal set necessarily results in a value of* $d^2_{\min} < 2$.

For arbitrary memory ν, by a straightforward extension of the procedure for memory one, it can be shown that the distance between any pair of length $\nu + 1$ paths beginning and ending at the same node (i.e., pairwise error events) is, analogously to Eq. (80), given by

$$d^2 \triangleq 1 - \frac{\mathrm{Re}\left\{\int_0^T s_0^*(t)\, s_{2^{\nu+1}-1}(t)\, dt\right\}}{(E_0 + E_{2^{\nu+1}-1})/2} \tag{85}$$

Thus, to achieve the maximum value $d^2_{\min} = 2$, we would need to choose $s_0(t) = -s_{2^{\nu+1}-1}(t)$, which produces $E_0 = E_{2^{\nu+1}-1}$. However, in view of the other forms [analogous to Eq. (84)] that Eq. (85) can be expressed as, it can also be shown that achieving $d^2_{\min} = 2$ also requires choosing $s_i(t) = -s_{2^{\nu+1}-1-i}(t)$, $i = 1, 2, \cdots, 2^\nu - 1$, which produces $E_i = E_{2^{\nu+1}-1-i}$, $i = 1, 2, \cdots, 2^\nu - 1$. Finally, using the energy conditions in Eq. (80), we arrive at the fact that $d^2_{\min} = 2$ can only be achieved when $E_0 = E_1 = E_2 = \cdots = E_{2^{\nu+1}-1} = E$, i.e., all signals have equal energy. Thus, we conclude that *for arbitrary memory, an unequal energy signal set necessarily results in a value of* $d^2_{\min} < 2$.

VI. Conclusion

It is possible to design constant-energy TCM signals that, when transmitted over the AWGN, achieve a significant improvement in out-of-band power performance relative to conventional modulation schemes, e.g., MSK, yet still achieve the maximum value of the minimum squared Euclidean distance and also have finite decoding delay. These bandwidth- and power-efficient signals can be implemented using a simple pulse-amplitude modulation (PAM)-based transmitter.

References

[1] Q. Li and B. E. Rimoldi, "Bandwidth-Efficient Trellis-Coded Modulation Scheme with Prescribed Decoding Delay," ISIT 1997, Ulm, Germany, June 29–July 4, 1997.

[2] G. D. Forney, Jr., "The Viterbi Algorithm," *Proc. IEEE*, vol. 61, no. 3, pp. 268–278, March 1973.

[3] B. E. Rimoldi, "A Decomposition Approach to CPM," *IEEE Trans. Inform. Theory*, vol. IT-34, pp. 260–270, May 1988.

[4] M. K. Simon, S. M. Hinedi, and W. C. Lindsey, *Digital Communication Techniques: Signal Design and Detection*, Englewood Cliffs, New Jersey: Prentice-Hall, Inc., 1995.

[5] M. K. Simon, "A Generalization of MSK-Type Signaling Based Upon Input Data Symbol Pulse Shaping," *IEEE Trans. Comm.*, vol. COM-24, no. 8, pp. 845–856, August 1976.

[6] F. Amoroso, "Pulse and Spectrum Manipulation in the MSK Format," *IEEE Trans. Comm.*, vol. COM-24, no. 3, pp. 381–384, March 1976.

[7] A. J. Viterbi and J. K. Omura, *Principles of Digital Communication and Coding*, New York: McGraw-Hill, Inc., 1979.